Journal Pre-proof

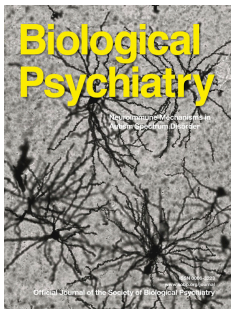

Computational modelling of EEG and fMRI paradigms indicates a consistent loss of pyramidal cell synaptic gain in schizophrenia

Rick A. Adams, Dimitris Pinotsis, Konstantinos Tsirlis, Leonhardt Unruh, Aashna Mahajan, Ana Montero Horas, Laura Convertino, Ann Summerfelt, Hemalatha Sampath, Xiaoming Michael Du, Peter Kochunov, Jie Lisa Ji, Grega Repovs, John D. Murray, Karl J. Friston, L Elliot Hong, Alan Anticevic

PII: S0006-3223(21)01499-2

DOI: https://doi.org/10.1016/j.biopsych.2021.07.024

Reference: BPS 14627

To appear in: *Biological Psychiatry*

Received Date: 31 March 2021

Revised Date: 29 July 2021

Accepted Date: 29 July 2021

Please cite this article as: Adams R.A, Pinotsis D., Tsirlis K., Unruh L., Mahajan A., Horas A.M., Convertino L., Summerfelt A., Sampath H., Du X.M., Kochunov P., Ji J.L., Repovs G., Murray J.D, Friston K.J, Hong L.E. & Anticevic A., Computational modelling of EEG and fMRI paradigms indicates a consistent loss of pyramidal cell synaptic gain in schizophrenia, *Biological Psychiatry* (2021), doi: https://doi.org/10.1016/j.biopsych.2021.07.024.

Computational modelling of EEG and fMRI paradigms indicates a consistent loss of pyramidal cell synaptic gain in schizophrenia

Rick A Adams[1,2,3,4]*, Dimitris Pinotsis[5,6], Konstantinos Tsirlis[1], Leonhardt Unruh[4], Aashna Mahajan[1], Ana Montero Horas[1], Laura Convertino[4], Ann Summerfelt[7], Hemalatha Sampath[7], Xiaoming Michael Du[7], Peter Kochunov[7], Jie Lisa Ji[3], Grega Repovs[8], John D Murray[3], Karl J Friston[9], L Elliot Hong[7], Alan Anticevic[3]

[1]Centre for Medical Image Computing and AI, University College London, 90 High Holborn, London, WC1V 6LJ, UK
[2]Max Planck-UCL Centre for Computational Psychiatry and Ageing Research, 10-12 Russell Square, London, WC1B 5EH, UK
[3]Department of Psychiatry, Yale University School of Medicine, 300 George Street, New Haven, CT 06511, USA
[4]Institute of Cognitive Neuroscience, University College London, 17 Queen Square, London, WC1N 3AZ, UK
[5]Centre for Mathematical Neuroscience and Psychology and Department of Psychology, City University of London, London, EC1V 0HB, UK
[6]The Picower Institute for Learning & Memory and Department of Brain and Cognitive Sciences, Massachusetts Institute of Technology, Cambridge, MA 02139, USA
[7]Department of Psychiatry, Maryland Psychiatric Research Center, University of Maryland School of Medicine, Baltimore, MD 21228, USA
[8]Department of Psychology, University of Ljubljana, 1000 Ljubljana, Slovenia
[9]The Wellcome Centre for Human Neuroimaging, University College London, 12 Queen Square, London, WC1N 3BG, UK

*corresponding author: rick.adams@ucl.ac.uk

Short title: Loss of pyramidal synaptic gain in schizophrenia

Schizophrenia; psychosis; dynamic causal model; mismatch negativity; auditory steady state; resting state

Abstract

Background

Diminished synaptic gain – the sensitivity of postsynaptic responses to neural inputs – may be a fundamental synaptic pathology in schizophrenia. Evidence for this is indirect, however. Furthermore, it is unclear whether pyramidal cells or interneurons (or both) are affected, or how these deficits relate to symptoms.

Methods

Participants with schizophrenia diagnoses (PScz, n=108), their relatives (n=57), and controls (n=107) underwent three electroencephalography (EEG) paradigms – resting, mismatch negativity, and 40 Hz auditory steady-state response – and resting functional magnetic resonance imaging. Dynamic causal modelling was used to quantify synaptic connectivity in cortical microcircuits.

Results

Classic group differences in EEG features between PScz and controls were replicated, including increased theta and other spectral changes (resting EEG), reduced mismatch negativity, and reduced 40 Hz power. Across all four paradigms, characteristic PScz data features were all best explained by models with greater self-inhibition (decreased synaptic gain), in pyramidal cells. Furthermore, disinhibition in auditory areas predicted abnormal auditory perception (and positive symptoms) in PScz, in three paradigms.

Conclusions

First, characteristic EEG changes in PScz in three classic paradigms are all attributable to the same underlying parameter change: greater self-inhibition in pyramidal cells. Second, psychotic symptoms in PScz relate to disinhibition in neural circuits. These findings are more commensurate with the hypothesis that in PScz, a primary loss of synaptic gain on pyramidal cells is then compensated by interneuron downregulation (rather than the converse). They further suggest that psychotic symptoms relate to this secondary downregulation.

Introduction

Reduced excitatory synaptic gain (i.e. decreased slope of the presynaptic input-postsynaptic response relationship) is believed to be a primary deficit in schizophrenia (1,2). This reduction may primarily affect pyramidal cells (1) or inhibitory interneurons (3). For example, loss of cortical interneuron markers (in *post mortem* studies of people with schizophrenia diagnoses, PScz) was originally thought to indicate a primary interneuron pathology, but recent work suggests these markers are activity-dependent, so their loss may reflect weaker pyramidal inputs (4). Decreased interneuron function in the disorder may thus be primary or a compensatory response to try to rebalance excitatory and inhibitory transmission in cortical circuits (5). These hypotheses are difficult to test *in vivo*, however.

Various mechanisms may reduce synaptic gain in schizophrenia: the most important is probably hypofunction of *N*-methyl-D-aspartate receptors (NMDARs) and their postsynaptic signalling cascade (1,2). Evidence for this comes from psychiatric genetics (6), magnetic resonance spectroscopy (MRS) imaging (7), neuropathological studies (4), and animal models (8), but of these, only MRS is performed in humans *in vivo*, and its glutamatergic measures are difficult to interpret. Other neuromodulatory dysfunctions in schizophrenia (e.g. reduced cortical dopamine (9) or muscarinic receptors (10)) can be assessed more directly using positron emission tomography (PET)), but MRS and PET are very indirect measures of synaptic gain.

An alternative way to investigate synaptic gain is using electroencephalography (EEG) paradigms such as the mismatch negativity (MMN, an auditory oddball paradigm (11)) and auditory steady-state response at 40 Hz (40 Hz ASSR, a paradigm inducing neural oscillations using a click train (12)), or in the 'resting state', measured with EEG (rsEEG) or functional magnetic resonance imaging (rsfMRI). PScz show robust reductions in 40 Hz ASSR (12) ($d \approx 0.6$) and MMN (11) ($d \approx 1$) responses, which may relate to diminished synaptic gain and decreased gain modulation (13) respectively, but these paradigms are not direct indices of synaptic gain.

Neural mass models of non-invasive data can be parameterised in terms of synaptic gain, and these parameters estimated, for example, using dynamic causal modelling (DCM) (14), furnishing model-based biomarkers (15,16). This has several advantages: it can estimate

subject-specific parameters, and can fit evoked (e.g. MMN) and induced (e.g. 40 Hz ASSR or resting) EEG responses and rsfMRI, and thus explain responses to different paradigms in terms of common synaptic parameters, such as gain or 'self-inhibition' on pyramidal cells or interneurons. (Although fMRI models cannot incorporate detailed microcircuit parameters, due to fMRI's coarse temporal resolution, they can assess local changes in excitability). Third, one can employ hierarchical modelling, e.g. using group-level parameters recursively to inform single-subject fits, for example, using Parametric Empirical Bayes (PEB) (17).

To date, DCM studies of PScz have used modest sample sizes and single paradigms, but have found reasonably consistent results, e.g. cortical disinhibition in EEG (13,18–20) and rsfMRI (21) and diminished contextual gain modulation (13,19,22). Nevertheless, foundational questions remain, including: Are well-replicated group differences between PScz and controls across paradigms all ascribable to the same model parameter(s)? How do symptoms in PScz relate to these parameters? Here, we address these questions using DCM across multiple EEG and fMRI paradigms, in PScz, controls, and first degree relatives.

Methods

Data were collected from PScz (n=107) recruited from outpatient clinics, first degree relatives (Rel, n=57) and controls (Con, n=108) recruited from media advertisements, who each underwent rsEEG, MMN, 40 Hz ASSR and rsfMRI paradigms, and recorded symptom and other measures. PScz and Con were well matched in terms of age (mean ±std 39.4 ±14.3 years and 39.4 ±13.9 years respectively), sex (59% and 68% male respectively) and smoking status (33% and 39% smokers respectively). PScz had mean BPRS scores of 14.4/49 for positive symptoms and 7.3/28 for negative symptoms (see Table S1). We first performed conventional analyses of group differences in data features for each paradigm. We then inferred the best explanations for these differences in terms of DCM parameters. Figure 1 summarises the analysis (excluding results).

We used the DCM canonical microcircuit neural mass model (Figure S1) to analyse the EEG paradigms: more details are given in the Results, with a full description in the Supplement. Model parameters include connectivity strengths between populations, self-inhibition (synaptic gain) in these populations, and membrane time constants and transmission delays. For the rsEEG, MMN and 40 Hz ASSR paradigms, we analysed group differences using conventional data features (event related potentials or power spectra). We then modelled either group-averaged data (rsEEG) or estimated subject-specific DCM parameters (MMN and 40 Hz ASSR). For rsfMRI, we only modelled the network generating the MMN (and 40 Hz ASSR, in part), for comparative purposes.

We used PEB to analyse group and individual differences in synaptic (model) parameters, with the exception of rsEEG, where characteristic group responses were modelled. We interpret greater 'self-inhibition' of pyramidal cells as an effective loss of pyramidal synaptic gain. Given known pathophysiology in PScz, NMDAR hypofunction seems the most likely explanation for loss of pyramidal gain, but other explanations are possible (see Supplement for further discussion).

Age, sex, smoking and chlorpromazine dose equivalent covariates did not significantly affect the results, unless otherwise stated. All *t*-tests were two-tailed, ranksum tests were used if distributions were skewed; none are Bonferroni-corrected unless stated.

Results

In rsEEG, PScz have altered power in θ, β and γ frequency bands

We first examined rsEEG power spectra by subtracting the 1/f gradient, noting that gradients did not differ between groups with eyes open or closed (P>0.2). The mean adjusted power spectra within the Con (n=98) and PScz (n=95) groups are shown in Figure 2A, for eyes closed (left) and open (right) conditions, with θ/α/β/γ frequency bands demarcated. A repeated measures ANOVA (between-subjects factor Group, within-subjects factors Eyes open/closed and Frequency band) demonstrated a significant interaction of Frequency*Group (F(3, 573)=6.59, P<0.001) but not of Eyes*Group (F(1, 191)=0.05, P=0.8) or of Frequency*Eyes*Group (F(3, 573)=0.4, P=0.8). We therefore averaged the power in each frequency band across eyes open and closed conditions, and performed Wilcoxon ranksum tests (as some distributions were skewed), Bonferroni-corrected for four frequency bands (Figure 2B). PScz had increased θ (Z=2.63, P(corr)=0.035), decreased β (Z=-2.77, P(corr)=0.022), and increased γ (Z=2.58, P(corr)=0.040), but unchanged α (Z=-1.32, P(corr)=0.75).

Increased pyramidal self-inhibition explains θ, β and γ changes in PScz

We used DCM's canonical microcircuit model – a biophysical model of interacting pyramidal, interneuron and spiny stellate populations (Figure 2C, left) – to identify the most likely synaptic pathology. To model power spectrum changes in PScz, we treated cortex as a single microcircuit in which specific parameters were changed in five plausible ways (Figure 2D, bottom): a loss of all microcircuit connectivity (Model 1), a loss of pyramidal connections to or from interneurons (Model 2), interneuron disinhibition (Model 3), increased interneuron self-inhibition (Model 4) and increased pyramidal cell self-inhibition (Model 5). Note that this model does not fit the large α peak.

Only Model 5 could explain the θ, β and γ changes seen in PScz (Figure 2D, upper row); Models 1 and 2 only reproduced the θ and β changes. Model 3 showed decreased β peak frequency, which was quantitatively lower in PScz but not statistically significant (Figure S2A).

MMN and P100 are reduced in both PScz and Rel

The MMN paradigm consisted of standard and duration-deviant tones. The 'mismatch amplitude' is the deviant–standard response in electrode Fz (11), which was reduced in both PScz and Rel around 200 ms (Figure 3A). There were no significant group differences in MMN latency between Con (mean ±std latency=194±34 ms) and Rel (196±45 ms, P=0.8) or PScz (202±44 ms, P=0.18). In the averaged deviant and standard waveforms (Figure S2B) PScz showed reduced response amplitudes around 50-100 ms in both, and – interestingly – an exaggerated mismatch-like response around 175 ms in the standard condition.

Smoothed sensor-level data were analysed using cluster-based statistics. Across Con and PScz, there was a strong mismatch effect, peaking at 198 ms (peak $P_{(FWE)}$<0.001, t(376)=11.23; Figure 3B), which was reduced in PScz (peak at 186 ms, $P_{(unc)}$<0.001, cluster $P_{(FWE)}$=0.010, t(376)=3.46) and in Rel (peak at 198 ms, $P_{(unc)}$<0.001, cluster $P_{(FWE)}$=0.011, t(268)=3.83; Figure 3C). Likewise, PScz had a reduced P100 response (peak at 82 ms, $P_{(FWE)}$=0.003, cluster $P_{(FWE)}$<0.001, t(376)=4.83), as did Rel, although this was only significant at an uncorrected peak threshold (peak at 94 ms, $P_{(unc)}$=0.001, cluster $P_{(FWE)}$=0.8, t(268)=3.02; Figure S2C).

DCM of MMN indicates increased frontal self-inhibition in PScz, but disinhibition in Broca's area relates to abnormal auditory percepts

We first used model comparison to establish whether it was best to fix or estimate various microcircuit parameters in the MMN analysis (see Supplement). We compared six models (Figure 3D): Model 6G estimates six connectivity (G) parameters, Models 4Ga-d consider subsets of these six, and Model 6G,D,T also estimates delays and time constants. Bayesian model selection preferred Model 6G (also in Con and PScz separately), with a protected exceedance probability of P=0.89 (Figure 3E, left). This model fitted most participants' data accurately (e.g. Figure S3A): a histogram of R^2 values is shown in Figure 3E (right) – the group mean R^2 was 0.73. R^2 were slightly higher in Con (mean=0.76 ±std=0.13) than in PScz (0.70±0.14; ranksum Z=3.12, P=0.0018) and Rel (0.71±0.15; ranksum Z=2.14, P=0.033) (Figure S3C).

We then used PEB to ask which parameters best explained group differences in the MMN: self-inhibition within areas or connections between areas. The reduced mismatch amplitude in PScz was best explained by increased self-inhibition in deviant – relative to standard – trials in L IFG (P>0.95) and R IFG (P>0.99; Figure 3F). Including chlorpromazine dose

equivalent covariates reduced the posterior probability to $P>0.75$, but age, sex and smoking had no effect. Conversely, there was no overall group effect (across both standards and deviants) of PScz on the microcircuit parameters (all $P<0.95$; Figure S4C, left) unless chlorpromazine dose equivalents were included as covariates: here, PScz showed greater superficial pyramidal self-inhibition in L and R IFG (both $P>0.99$; Figure S4C, middle and right) and reduced interneuron self-inhibition throughout ($P>0.95$). Rel did not show effects of $P>0.95$ in either analysis.

In PScz, the auditory perceptual abnormalities 'state' measure was associated with disinhibition in L IFG ($P>0.99$) – within Broca's area – but increased self-inhibition in R IFG ($P>0.95$) in the mismatch contrast (Figure 3G). Historical auditory perceptual abnormalities (the 'trait' measure) showed similar effects but at lower posterior probability ($P>0.75$, not shown).

PScz had reduced γ power and peak frequency in 40 Hz ASSR, and Rel reduced γ power

We next considered induced responses during auditory steady-state stimulation. Group-averaged 40 Hz ASSR are shown in Figure 4A, and the distributions of participants' peak γ (35-45 Hz) frequencies in Figure 4B. PScz had slightly reduced γ peak frequency: mean peak frequencies (following subtraction of the 1/f gradient: Figure S2E) were Con=40.2 Hz (std 1.7), PScz=39.5 Hz (std 1.7; $t(184)=2.67$, $P(\text{corr})=0.016$) and Rel=39.9 Hz (std 2.1; $t(132)=1.03$, $P=0.3$). Adjusted time-frequency plots are shown in Figure 4C (and raw time frequency data in Figure S2F): Con showed a robust increase in ~40 Hz power around 100 ms, which is diminished in PScz and Rel ($P<0.05$ *t*-tests at each frequency and timepoint are circled on the middle and right plots, for Con vs PScz and Con vs Rel in black and PScz vs Rel in white: this many differences are unlikely due to chance – Con vs PScz and Con vs Rel both $P<0.001$, PScz vs Rel $P=0.006$, permutation tests). Maximum ASSR γ power correlated with MMN amplitude in PScz ($r=0.28$, $P(\text{corr})=0.029$) but not in Con ($r=0.04$, $P=0.7$) or Rel ($r=0.14$, $P=0.4$).

40 Hz ASSR DCM suggests a loss of pyramidal input to interneurons in PScz and Rel, and greater self-inhibition in PScz

The peak cortical source – closest to A1 – was [50 -12 4], hence bilateral sources at [±50 -12 4] were used as priors for reconstruction of virtual electrode data: the DCM comprised these

bilateral sources and their thalamic drive (Figure 4D). Empirical priors for several parameters were used to optimise model fit (Figure S1A). Bayesian model comparison between the Full model (containing empirical priors for the contribution of spiny stellate cells to measured signals, the neural activation function, and synaptic time constants) and models with standard priors for these parameters showed the Full model was superior (Figure 4E, left). The 40 Hz thalamic drive was modelled using a Gaussian bump function of width w≤4 Hz (see Supplement): this width performed better than a narrower bump of 1 Hz (Model -w, Figure 4E). Model fits for the winning model were reasonable (Figure S3B; mean R^2=0.53). Group differences in R^2 were not detected (Figure S3C, ranksum tests: all P>0.1).

We performed group comparisons with PEB using schizophrenia 'genetic risk' (PScz+Rel > Con) and 'diagnosis' (PScz > Rel) as explanatory variables (13,19), instead of PScz > Con and Rel > Con comparisons (as in the MMN analysis). This was because the group differences in data features were less marked in the 40 Hz ASSR, and there were substantial differences between Rel and Con parameters, only some of which were shared by PScz (Figure S6B). The 'genetic risk' effect was an increased conduction delay in L A1 (P>0.95; Figure 4F), and reduced superficial pyramidal (sp) to inhibitory interneuron (ii) connectivity (P>0.99; Figure 4G, left). The schizophrenia 'diagnosis' effect was increased superficial pyramidal self-inhibition in bilateral A1 in PScz (both P>0.99; Figure 4G, right).

40 Hz ASSR DCM links abnormal auditory percepts to A1 disinhibition in PScz

In PScz, the auditory perceptual abnormalities 'trait' measure related to a disinhibited sp-ii-sp circuit, i.e. increased sp-ii (P>0.99) and reduced ii-sp connectivity (P>0.99), also greater self-inhibition in L A1 (P>0.99; Figure 4H). The auditory 'state' measure had similar associations but at lower posterior probability (P>0.95 for sp-ii, P>0.75 for ii-sp and sp-sp, not shown).

rsfMRI DCM of the MMN circuit finds increased self-inhibition in IFG in PScz and Rel

We then analysed effective connectivity within the 'MMN network' during rsfMRI, i.e. the Glasser parcellation areas (in the rsfMRI data) based on the MMN source locations (see Supplement): bilateral A1, A4 and 44 (Figure 1). The microcircuit model for fMRI data is simpler than the neural mass models used for EEG; however, they retain inhibitory self-connections. Model fits were accurate: R^2s were >0.7 in all groups, with no group differences (Figure S3C, ranksum tests: all P>0.05).

In PEB analysis, PScz showed increased self-inhibition in L and R IFG (P>0.99 and P>0.95 respectively; Figure 5A). These effects were robust to age, sex, and smoking covariates (and to the removal of the 10 participants with the lowest rsfMRI signal to noise ratio: 8 PScz and 2 Con; both P>0.95). These effects did not survive addition of chlorpromazine dose equivalents (L IFG self-inhibition fell to P>0.75). However, Rel > Con showed the same increase in self-inhibition in bilateral IFG (both P>0.95, Figure 5B). This group difference did not survive addition of the age covariate: Rel were older than Con (Rel mean age=45.4 ±16.6 years, Con mean age=39.4 ±14.3 years; $t(162)=2.4$, $P=0.02$). These differences were not detected using conventional functional connectivity analyses (that cannot assess self-inhibition) or analyses of regional variance (see Figures S6B to S6E and Supplement for further discussion).

rsfMRI DCM reveals relationships of positive symptoms to cortical disinhibition in PScz

PEB analysis within PScz found that 'trait' auditory perceptual abnormalities were associated with increased self-inhibition in L and R IFG (both P>0.99, Figure 5C, left). Conversely, 'state' auditory perceptual abnormalities were associated with disinhibition in R A1 (P>0.95) and L A1 and STG (both P>0.99), and of STG-A1 backward connectivity bilaterally (both P>0.99; Figure 5C, right).

Similarly, BPRS positive symptoms (including age, sex, smoking and negative symptoms covariates) were associated with decreased self-inhibition everywhere except R STG (all P>0.99 except L IFG and R A1, both P>0.95) and stronger forward connections everywhere except R Al-STG (all P>0.99; Figure 5D, left). Interestingly, BPRS negative symptoms (including age, sex, smoking and positive symptom covariates) were associated with decreased self-inhibition in all the temporal – but not frontal – nodes (all P>0.99; Figure 5D, right).

Note that many rsfMRI results were lost if global signal regression was not performed (Supplementary Results, Figure S7).

Self-inhibition findings in PScz across EEG and rsfMRI paradigms are similar

In summary, we found clear evidence for increased self-inhibition (evidence of reduced synaptic gain) in PScz (Figure 6A) in all data modalities and paradigms. However,

disinhibition within auditory areas was associated with auditory perceptual abnormalities within PScz (Figure 6B). A sensitivity analysis (see Supplement) confirmed that increased superficial pyramidal self-inhibition best reproduced the key data features of the MMN (i.e. decreased MMN amplitude but unchanged latency; Figure S8A) and – along with loss of sp-ii connectivity – the decreased 40 Hz ASSR (Figure S8B). Evidence for within-subject correlations in self-inhibition parameters across paradigms was weak, however (see Supplementary Results, Figure S9).

Discussion

Dynamic causal modelling of EEG and fMRI produced two key cross-paradigm findings. First, well-established effects in rsEEG (23), MMN (11) and 40 Hz ASSR (12) paradigms in PScz were replicated and all could be explained by increased self-inhibition in (superficial) pyramidal cells. Likewise, PScz also showed an increase in prefrontal self-inhibition – similar to the MMN – in rsfMRI (Figure 6A). This strongly favours the hypothesis that there is diminished synaptic gain on pyramidal cells (1,2,5), over the hypothesis of diminished synaptic gain on interneurons (3), in this sample of PScz with established illness.

Second, abnormal auditory percepts in PScz was associated with *decreased* self-inhibition in auditory areas selectively, across three paradigms (Figure 6B). This is consistent with 40 Hz ASSR γ power (24) (and phase locking of auditory γ (25)) correlating positively with auditory symptoms, despite being reduced in PScz overall (as in the visual domain (26)), and with hallucinations and psychotic-like experiences relating to decreased self-inhibition in IFG across the psychosis spectrum (27). Positive symptoms were also associated with disinhibition in the rsfMRI analysis (Figure 5D). These opposing effects of group and symptoms on self-inhibition (28) – and also on cortical glutamate (29) – support the hypothesis (1,5) that decreased synaptic gain (NMDAR hypofunction in particular) is compensated by allostatic disinhibition of pyramidal cells (i.e. interneuron downregulation) and, furthermore, indicate that psychotic symptoms result from this disinhibitory rebalancing of excitatory and inhibitory transmission.

In rsEEG, increased θ power in PScz is a well-established finding (23,30). A 'U-shaped' change in spectral power (here, increased θ, decreased β, increased γ), has been seen several times across θ, α and β frequencies (23). Increases (not decreases) in α and β in PScz have been seen in eyes open rsEEG (30,31), but in unnormalised data: prior to subtracting the 1/f gradient, β power was numerically higher in our sample of PScz too. This speaks to the importance of distinguishing band-specific changes from changes in 1/f slope, which itself is increased by lower excitation:inhibition ratio (32,33). Of note, low γ (30-45 Hz) power is typically reduced in PScz with longstanding diagnoses (34), but we lacked illness duration information.

Decreased mismatch amplitude in PScz (and especially in chronic PScz (35)) is well-documented (11), and we found an effect of similar size in Rel – larger than is typical (35). Underlying this effect, we found deviant stimuli decrease self-inhibition in IFG in Con, but not in PScz: recapitulating other DCM studies (13,22). The mismatch amplitude rarely correlates with hallucinations in PScz (e.g. in only 3/22 studies (11)), but we found abnormal auditory percepts related to (condition-specific) disinhibition in L IFG – Broca's area. Traditional MMN analysis (using electrode Fz) might miss this lateralised effect. Nevertheless, there are reports of left-lateralised associations of hallucinations (including IFG) with auditory oddball responses in PScz (36).

In the 40 Hz ASSR, PScz showed decreased γ power and peak frequency, and Rel decreased power (as elsewhere (12,20,37)). DCM indicated that diminished pyramidal connectivity to interneurons (and greater transmission delay) was common to both PScz and Rel, but loss of pyramidal gain was unique to PScz (Figure 4G). Others have modelled 40 Hz ASSR in PScz by increasing interneuron time constants (38): this reproduced a concurrent increase in 20 Hz power in PScz (38), which was not observed in our data. We assumed time constants did not differ in PScz in the ASSR or MMN, and estimated connectivity parameters – and delays, in the ASSR – instead (these can be regarded as synaptic rate constants).

A previous rsfMRI DCM analysis in PScz found disinhibition in anterior cingulate cortex (21), rather than increased self-inhibition in bilateral IFG (Figure 5A). This recalls a pattern of altered intra-prefrontal functional connectivity in early PScz (39): increased connectivity of medial areas and more modest decreases in connectivity in lateral areas. Prefrontal hyperconnectivity correlated positively with positive symptoms (39). We similarly found positive symptoms were associated with disinhibition in bilateral IFG, and also A1 (Figure 5D, left). This relationship echoes findings that increased functional connectivity of primary sensory areas (to thalamus) correlates with PANSS scores (40), and that increased A1 rsfMRI autocorrelation (a result of reduced self-inhibition) in PScz relates to auditory hallucinations (28) (c.f. Figure 5C, right). Our results have commonalities with a spectroscopy mega-analysis that correlated positive symptoms to frontal and negative symptoms to temporal glutamate concentrations (29) (c.f. Figure 5D). Thus symptoms may depend not just on connectivity between nodes, but on synaptic gain within nodes: modelling is key to disambiguating these possibilities.

More data are required to draw firm conclusions about the Rel group. In the MMN, no effects exceeded $P>0.95$ despite Rel's similar data features to PScz. In the 40 Hz ASSR, pyramidal self-inhibition was reduced in Rel (Figure S5B), not increased. In the rsfMRI however, Rel showed comparable IFG self-inhibition increases to PScz (Figure 5B).

A crucial question is what changes in 'self-inhibition' mean: changes in synaptic gain, or reciprocal coupling with interneurons? Our interpretation of self-inhibition changes is guided by known pathophysiology in PScz: i.e. given cortical synaptic gain is decreased (e.g. reduced function of NMDA (1,2,6), dopamine 1 (9) and muscarinic (10) receptors), and inhibitory interneurons downregulated (4,5), then the most logical interpretation of increases and decreases in pyramidal self-inhibition are diminished pyramidal synaptic gain (41,42) and decreased interneuron function, respectively. ('Gain' in the neural mass model is discussed in detail in the Supplement.) If the fundamental pathology in PScz were a loss of synaptic gain on interneurons, one would expect to see consistent group effects of increased interneuron self-inhibition and/or decreased pyramidal self-inhibition: neither of which were found.

Regarding potential causes of reduced synaptic gain, some PScz data features imply NMDAR hypofunction. In rsEEG, increased γ follows NMDAR antagonism (43), e.g. using ketamine (which also suppresses β) (44) or in NMDAR encephalitis (which also increases θ) (15,45). In contrast, LSD and psilocybin do not increase θ (46), and dopamine 2 antagonists potentiate α and β (47,48). The 40 Hz ASSR is sensitive to NMDAR function (49) (but also cholinergic (50), dopaminergic (51) and serotonergic (52) manipulations): the latter do not affect the MMN, however, which is quite specific to NMDAR function (11). Ketamine also reduces rsfMRI functional connectivity of IFG and auditory cortices (53). Antipsychotic dose covariates weakened the PScz MMN condition-specific effects (Figure 3F) but strengthened the overall MMN effects (Figure S4C); they also weakened the PScz rsfMRI effects, but similar rsfMRI effects emerged in unmedicated Rel (Figure 5). Overall, these findings resemble NMDAR hypofunction, and seem unlikely to be medication-induced.

Several limitations are addressable: given pathophysiology is dynamic in PScz (1), and that subgroups may exist (54), larger datasets should be analysed, containing more early course (and preferably unmedicated) PScz. Notably, even the latter show reductions ($d>1$) in cortical glutamate (55), consistent with the idea that pyramidal cell hypofunction – rather than

disinhibition – is primary in PScz. DCM models with explicitly parameterised NMDA (and other) receptor conductances (15) can explore 'self-inhibition' in more detail, and across more cortical areas.

In conclusion, we found consistently increased self-inhibition (i.e. diminished synaptic gain) in PScz, especially in frontal areas, but disinhibition – in auditory areas in particular – correlated with auditory perceptual abnormalities. Psychotic symptoms may therefore be caused by interneuronal downregulation that restores cortical 'excitation/inhibition balance' in PScz. These complex processes may explain why successful glutamatergic treatments for PScz are elusive, and why such treatments may have narrow therapeutic windows (56) or depend on illness stage (57).

Acknowledgements

We are very grateful to numerous colleagues who provided guidance in DCM and statistics, including Vladimir Litvak, Peter Zeidman, Rosalyn Moran, Adeel Razi, Amirhossein Jafarian, Marta Garrido and Jon Roiser. RAA is an MRC Skills Development Fellow (MR/S007806/1) and has been supported by a UCL Bogue Research Fellowship, the Academy of Medical Sciences (AMS-SGCL13-Adams), the National Institute of Health Research (CL-2013-18-003), and the NIHR UCLH Biomedical Research Centre. GR is funded by Slovenian Research Agency grants J7-8275 and P3-0338. JDM is funded by NIH grant MH112746. KJF was funded by the Wellcome Trust (Ref: 088130/Z/09/Z). A preprint of this paper was posted to medRxiv (doi: 10.1101/2021.01.07.21249389).

Author contributions

RAA conceived the project, conducted or supervised all analyses, and wrote the paper. DP and KT developed analysis code and conducted some analyses. LU, AM, AMH, LC and JLJ assisted with analysis. AS, XMD, HS and PK collected and curated the data. GR developed analysis code, assisted with analysis, and contributed to the paper. JDM contributed to the paper. KJF developed analysis code, assisted with analysis, and contributed to the paper. LEH collected the data and contributed to the paper. AA supervised the project and contributed to the paper.

Competing interests

Grega Repovš consults for and holds equity in RBNC Therapetics. JLJ, JDM and AA consult for RBNC (formerly BlackThorn Therapeutics) and are listed as co-inventors on the following pending patent: Anticevic A, Murray JD, Ji JL: Systems and Methods for Neuro-Behavioral Relationships in Dimensional Geometric Embedding (N-BRIDGE), PCT International Application No. PCT/US2119/022110, filed March 13, 2019. JDM holds stock in BlackThorn Therapeutics. LEH has received or plans to receive research funding or

consulting fees on research projects from Mitsubishi, Your Energy Systems LLC, Neuralstem, Taisho, Heptares, Pfizer, Luye Pharma, Sound Pharma, Takeda, and Regeneron. AA is also a SAB member for BlackThorn Therapeutics. All other authors report no biomedical financial interests or potential conflicts of interest.

References

1. Krystal JH, Anticevic A, Yang GJ, Dragoi G, Driesen NR, Wang X-J, Murray JD (2017): Impaired Tuning of Neural Ensembles and the Pathophysiology of Schizophrenia: A Translational and Computational Neuroscience Perspective. *Biol Psychiatry* 81: 874–885.

2. Stephan KE, Friston KJ, Frith CD (2009): Dysconnection in schizophrenia: from abnormal synaptic plasticity to failures of self-monitoring. *Schizophr Bull* 35: 509–527.

3. Lewis DA, Hashimoto T, Volk DW (2005): Cortical inhibitory neurons and schizophrenia. *Nat Rev Neurosci* 6: 312–324.

4. Chung DW, Fish KN, Lewis DA (2016): Pathological Basis for Deficient Excitatory Drive to Cortical Parvalbumin Interneurons in Schizophrenia. *Am J Psychiatry* 173: 1131–1139.

5. Dienel SJ, Lewis DA (2019): Alterations in cortical interneurons and cognitive function in schizophrenia. *Neurobiol Dis* 131: 104208.

6. Hall J, Trent S, Thomas KL, O'Donovan MC, Owen MJ (2015): Genetic risk for schizophrenia: convergence on synaptic pathways involved in plasticity. *Biol Psychiatry* 77: 52–58.

7. Poels EMP, Kegeles LS, Kantrowitz JT, Javitt DC, Lieberman JA, Abi-Dargham A, Girgis RR (2014): Glutamatergic abnormalities in schizophrenia: a review of proton MRS findings. *Schizophr Res* 152: 325–332.

8. Neill JC, Barnes S, Cook S, Grayson B, Idris NF, McLean SL, *et al.* (2010): Animal models of cognitive dysfunction and negative symptoms of schizophrenia: focus on NMDA receptor antagonism. *Pharmacol Ther* 128: 419–432.

9. Slifstein M, van de Giessen E, Van Snellenberg J, Thompson JL, Narendran R, Gil R, *et al.* (2015): Deficits in prefrontal cortical and extrastriatal dopamine release in

schizophrenia: a positron emission tomographic functional magnetic resonance imaging study. *JAMA Psychiatry* 72: 316–324.

10. Scarr E, Cowie TF, Kanellakis S, Sundram S, Pantelis C, Dean B (2009): Decreased cortical muscarinic receptors define a subgroup of subjects with schizophrenia. *Mol Psychiatry* 14: 1017–1023.

11. Umbricht D, Krljes S (2005): Mismatch negativity in schizophrenia: a meta-analysis. *Schizophrenia Research* 76: 1–23.

12. Thuné H, Recasens M, Uhlhaas PJ (2016): The 40-Hz Auditory Steady-State Response in Patients With Schizophrenia: A Meta-analysis. *JAMA Psychiatry* 73: 1145–1153.

13. Ranlund S, Adams RA, Díez Á, Constante M, Dutt A, Hall M-H, *et al.* (2016): Impaired prefrontal synaptic gain in people with psychosis and their relatives during the mismatch negativity. *Hum Brain Mapp* 37: 351–365.

14. Stephan KE, Schlagenhauf F, Huys QJM, Raman S, Aponte EA, Brodersen KH, *et al.* (2017): Computational neuroimaging strategies for single patient predictions. *Neuroimage* 145: 180–199.

15. Symmonds M, Moran CH, Leite MI, Buckley C, Irani SR, Stephan KE, *et al.* (2018): Ion channels in EEG: isolating channel dysfunction in NMDA receptor antibody encephalitis. *Brain* 141: 1691–1702.

16. Shaw AD, Hughes LE, Moran R, Coyle-Gilchrist I, Rittman T, Rowe JB (2019): In Vivo Assay of Cortical Microcircuitry in Frontotemporal Dementia: A Platform for Experimental Medicine Studies. *Cereb Cortex*. https://doi.org/10.1093/cercor/bhz024

17. Friston KJ, Litvak V, Oswal A, Razi A, Stephan KE, van Wijk BCM, *et al.* (2016): Bayesian model reduction and empirical Bayes for group (DCM) studies. *Neuroimage* 128: 413–431.

18. Dima D, Frangou S, Burge L, Braeutigam S, James AC (2012): Abnormal intrinsic and extrinsic connectivity within the magnetic mismatch negativity brain network in schizophrenia: A preliminary study. *Schizophr Res* 135: 23–27.

19. Díez Á, Ranlund S, Pinotsis D, Calafato S, Shaikh M, Hall M-H, *et al.* (2017): Abnormal frontoparietal synaptic gain mediating the P300 in patients with psychotic disorder and their unaffected relatives. *Hum Brain Mapp* 38: 3262–3276.

20. Shaw AD, Knight L, Freeman TCA, Williams GM, Moran RJ, Friston KJ, *et al.* (2020): Oscillatory, Computational, and Behavioral Evidence for Impaired GABAergic Inhibition in Schizophrenia. *Schizophr Bull* 46: 345–353.

21. Bastos-Leite AJ, Ridgway GR, Silveira C, Norton A, Reis S, Friston KJ (2015): Dysconnectivity within the default mode in first-episode schizophrenia: a stochastic dynamic causal modeling study with functional magnetic resonance imaging. *Schizophr Bull* 41: 144–153.

22. Fogelson N, Litvak V, Peled A, Fernandez-del-Olmo M, Friston K (2014): The functional anatomy of schizophrenia: A dynamic causal modeling study of predictive coding. *Schizophr Res* 158: 204–212.

23. Boutros NN, Arfken C, Galderisi S, Warrick J, Pratt G, Iacono W (2008): The status of spectral EEG abnormality as a diagnostic test for schizophrenia. *Schizophr Res* 99: 225–237.

24. Puvvada KC, Summerfelt A, Du X, Krishna N, Kochunov P, Rowland LM, *et al.* (2018): Delta Vs Gamma Auditory Steady State Synchrony in Schizophrenia. *Schizophr Bull* 44: 378–387.

25. Spencer KM, Niznikiewicz MA, Nestor PG, Shenton ME, McCarley RW (2009): Left auditory cortex gamma synchronization and auditory hallucination symptoms in schizophrenia. *BMC Neurosci* 10: 85.

26. Spencer KM, Nestor PG, Perlmutter R, Niznikiewicz MA, Klump MC, Frumin M, *et al.* (2004): Neural synchrony indexes disordered perception and cognition in schizophrenia. *Proc Natl Acad Sci USA* 101: 17288–17293.

27. Dzafic I, Larsen KM, Darke H, Pertile H, Carter O, Sundram S, Garrido MI (2021): Stronger Top-Down and Weaker Bottom-Up Frontotemporal Connections During Sensory Learning Are Associated With Severity of Psychotic Phenomena. *Schizophr Bull*. https://doi.org/10.1093/schbul/sbaa188

28. Wengler K, Goldberg AT, Chahine G, Horga G (2020): Distinct hierarchical alterations of intrinsic neural timescales account for different manifestations of psychosis. *Elife* 9. https://doi.org/10.7554/eLife.56151

29. Merritt K, McGuire PK, Egerton A, 1H-MRS in Schizophrenia Investigators, Aleman A, Block W, *et al.* (2021): Association of Age, Antipsychotic Medication, and Symptom Severity in Schizophrenia With Proton Magnetic Resonance Spectroscopy Brain Glutamate Level: A Mega-analysis of Individual Participant-Level Data. *JAMA Psychiatry*. https://doi.org/10.1001/jamapsychiatry.2021.0380

30. Narayanan B, O'Neil K, Berwise C, Stevens MC, Calhoun VD, Clementz BA, *et al.* (2014): Resting state electroencephalogram oscillatory abnormalities in schizophrenia and psychotic bipolar patients and their relatives from the bipolar and schizophrenia network on intermediate phenotypes study. *Biol Psychiatry* 76: 456–465.

31. Newson JJ, Thiagarajan TC (2018): EEG Frequency Bands in Psychiatric Disorders: A Review of Resting State Studies. *Front Hum Neurosci* 12: 521.

32. Gao R, Peterson EJ, Voytek B (2017): Inferring synaptic excitation/inhibition balance from field potentials. *Neuroimage* 158: 70–78.

33. Peterson EJ, Rosen BQ, Campbell AM, Belger A, Voytek B (2017): 1/f neural noise is a better predictor of schizophrenia than neural oscillations. *bioRxiv* 113449.

34. Grent-’t-Jong T, Gross J, Goense J, Wibral M, Gajwani R, Gumley AI, *et al.* (2018): Resting-state gamma-band power alterations in schizophrenia reveal E/I-balance abnormalities across illness-stages. *Elife* 7. https://doi.org/10.7554/eLife.37799

35. Erickson MA, Ruffle A, Gold JM (2016): A Meta-Analysis of Mismatch Negativity in Schizophrenia: From Clinical Risk to Disease Specificity and Progression. *Biol Psychiatry* 79: 980–987.

36. Taylor JA, Larsen KM, Garrido MI (2020): Multi-dimensional predictions of psychotic symptoms via machine learning. *Hum Brain Mapp*. https://doi.org/10.1002/hbm.25181

37. Hong LE, Summerfelt A, McMahon R, Adami H, Francis G, Elliott A, *et al.* (2004): Evoked gamma band synchronization and the liability for schizophrenia. *Schizophr Res* 70: 293–302.

38. Vierling-Claassen D, Siekmeier P, Stufflebeam S, Kopell N (2008): Modeling GABA alterations in schizophrenia: a link between impaired inhibition and altered gamma and beta range auditory entrainment. *J Neurophysiol* 99: 2656–2671.

39. Anticevic A, Hu X, Xiao Y, Hu J, Li F, Bi F, *et al.* (2015): Early-course unmedicated schizophrenia patients exhibit elevated prefrontal connectivity associated with longitudinal change. *J Neurosci* 35: 267–286.

40. Anticevic A, Cole MW, Repovs G, Murray JD, Brumbaugh MS, Winkler AM, *et al.* (2014): Characterizing thalamo-cortical disturbances in schizophrenia and bipolar illness. *Cereb Cortex* 24: 3116–3130.

41. Bygrave AM, Kilonzo K, Kullmann DM, Bannerman DM, Kätzel D (2019): Can N-Methyl-D-Aspartate Receptor Hypofunction in Schizophrenia Be Localized to an Individual Cell Type? *Front Psychiatry* 10: 835.

42. Stein H, Barbosa J, Rosa-Justicia M, Prades L, Morató A, Galan-Gadea A, *et al.* (2020): Reduced serial dependence suggests deficits in synaptic potentiation in anti-NMDAR encephalitis and schizophrenia. *Nat Commun* 11: 4250.

43. Lemercier CE, Holman C, Gerevich Z (2017): Aberrant alpha and gamma oscillations ex vivo after single application of the NMDA receptor antagonist MK-801. *Schizophr Res* 188: 118–124.

44. Rivolta D, Heidegger T, Scheller B, Sauer A, Schaum M, Birkner K, *et al.* (2015): Ketamine Dysregulates the Amplitude and Connectivity of High-Frequency Oscillations in Cortical-Subcortical Networks in Humans: Evidence From Resting-State Magnetoencephalography-Recordings. *Schizophr Bull* 41: 1105–1114.

45. Gitiaux C, Simonnet H, Eisermann M, Leunen D, Dulac O, Nabbout R, *et al.* (2013): Early electro-clinical features may contribute to diagnosis of the anti-NMDA receptor encephalitis in children. *Clin Neurophysiol* 124: 2354–2361.

46. Pallavicini C, Vilas MG, Villarreal M, Zamberlan F, Muthukumaraswamy S, Nutt D, *et al.* (2019): Spectral signatures of serotonergic psychedelics and glutamatergic dissociatives. *Neuroimage* 200: 281–291.

47. Ongini E, Bo P, Dionisotti S, Trampus M, Savoldi F (1992): Effects of remoxipride, a dopamine D-2 antagonist antipsychotic, on sleep-waking patterns and EEG activity in rats and rabbits. *Psychopharmacology (Berl)* 107: 236–242.

48. Sebban C, Zhang XQ, Tesolin-Decros B, Millan MJ, Spedding M (1999): Changes in EEG spectral power in the prefrontal cortex of conscious rats elicited by drugs interacting with dopaminergic and noradrenergic transmission. *Br J Pharmacol* 128: 1045–1054.

49. Sivarao DV (2015): The 40-Hz auditory steady-state response: a selective biomarker for cortical NMDA function. *Ann N Y Acad Sci* 1344: 27–36.

50. Sivarao DV, Frenkel M, Chen P, Healy FL, Lodge NJ, Zaczek R (2013): MK-801 disrupts and nicotine augments 40 Hz auditory steady state responses in the auditory cortex of the urethane-anesthetized rat. *Neuropharmacology* 73: 1–9.

51. Albrecht MA, Price G, Lee J, Iyyalol R, Martin-Iverson MT (2013): Dexamphetamine selectively increases 40 Hz auditory steady state response power to target and nontarget stimuli in healthy humans. *J Psychiatry Neurosci* 38: 24–32.

52. Nissen TD, Laursen B, Viardot G, l'Hostis P, Danjou P, Sluth LB, *et al.* (2020): Effects of Vortioxetine and Escitalopram on Electroencephalographic Recordings - A Randomized, Crossover Trial in Healthy Males. *Neuroscience* 424: 172–181.

53. Adhikari BM, Dukart J, Hipp JF, Forsyth A, McMillan R, Muthukumaraswamy SD, *et al.* (2020): Effects of ketamine and midazolam on resting state connectivity and comparison with ENIGMA connectivity deficit patterns in schizophrenia. *Hum Brain Mapp* 41: 767–778.

54. Clementz BA, Sweeney JA, Hamm JP, Ivleva EI, Ethridge LE, Pearlson GD, *et al.* (2016): Identification of Distinct Psychosis Biotypes Using Brain-Based Biomarkers. *Am J Psychiatry* 173: 373–384.

55. Jeon P, Limongi R, Ford SD, Mackinley M, Dempster K, Théberge J, Palaniyappan L (2021): Progressive Changes in Glutamate Concentration in Early Stages of Schizophrenia: A Longitudinal 7-Tesla MRS Study. *Schizophrenia Bulletin Open* 2. https://doi.org/10.1093/schizbullopen/sgaa072

56. Javitt DC (2016): Bitopertin in schizophrenia: glass half full? *Lancet Psychiatry* 3: 1092–1093.

57. Kinon BJ, Millen BA, Zhang L, McKinzie DL (2015): Exploratory analysis for a targeted patient population responsive to the metabotropic glutamate 2/3 receptor agonist pomaglumetad methionil in schizophrenia. *Biol Psychiatry* 78: 754–762.

58. Garrido MI, Kilner JM, Stephan KE, Friston KJ (2009): The mismatch negativity: a review of underlying mechanisms. *Clin Neurophysiol* 120: 453–463.

59. Shaw AD, Moran RJ, Muthukumaraswamy SD, Brealy J, Linden DE, Friston KJ, Singh KD (2017): Neurophysiologically-informed markers of individual variability and pharmacological manipulation of human cortical gamma. *Neuroimage* 161: 19–31.

Figure 1 – An overview of the analysis.

This schematic illustrates the key steps in the preprocessing of the EEG (resting state, mismatch negativity and 40 Hz auditory steady-state response) and resting state fMRI paradigms, and their subsequent analysis using dynamic causal modelling (DCM) and parametric empirical Bayes (PEB). Simplified depictions of the paradigms are shown in the first column (see Supplement for details), with group differences in EEG data features in the second column (first three rows), and DCM in the third column. The EEG data Con vs PScz group differences are (from first to third rows) in rsEEG θ, β, and γ frequency band power (Figure 2A), MMN responses (Figure 3A) and 40 Hz ASSR power (Figure 4C). The second column of the final row (rsfMRI) shows the Glasser parcellation areas A1 (middle), A4 (left) and 44 (right) containing the MMN sources A1, STG and IFG (respectively): these were used as nodes in the rsfMRI analysis, so that results could be compared across data modalities. Key preprocessing and analysis steps are described below the illustrations. DCM for EEG uses a cortical microcircuit model, shown on the left in the third column (also see Figure 2C). It contains superficial and deep pyramidal cells (blue triangles), inhibitory interneurons (red circle) and spiny stellate cells (green star). The lower three DCM illustrations include macroscopic model structures, i.e. the cortical areas involved: primary auditory cortex (A1), superior temporal gyrus (STG) and inferior frontal gyrus (IFG) (58). In the rsEEG analysis (top row), a ‘single area’ DCM was used to reproduce power spectra characteristic of each group. In the remaining paradigms, models were fitted to the data and PEB was used to analyze group and individual differences: the final column depicts an example analysis (from Figure 3F) of group differences in DCM parameters between Con and PScz in the MMN.

Figure 2 – rsEEG results, DCM model structure and rsEEG simulations.

A – The mean normalised eyes closed and eyes open rsEEG power spectra (±s.e.m.) across all channels for Con (n=98; blue) and PScz (n=95; red) groups, divided into four frequency bands (dotted lines): θ (3-7 Hz), α (8-14 Hz), β (15-30 Hz) and γ (>31 Hz).

B – Group comparisons in mean power across both eyes closed and eyes open conditions in the θ, α, β and γ bands are shown. The box plots show the mean, s.e.m. and std. *P* values are Bonferroni-corrected for four comparisons.

C – The EEG DCMs used the current version of the canonical microcircuit model (59) (also see Figure S1A). This microcircuit (shown left) consists of superficial and deep pyramidal cells (sp and dp), inhibitory interneurons (ii), and spiny stellate (ss) cells. They are interconnected with excitatory (arrowheads) and inhibitory (beads) connections; their self-inhibitory connections parameterize their responsiveness to their inputs, i.e. synaptic gain. In EEG DCM, each modelled cortical area contains a microcircuit (middle); fMRI DCM uses a much simpler neuronal model. Both DCMs have self-inhibition parameters (round grey beads) which – in the EEG case – inhibit superficial pyramidal cells specifically. A schematic DCM diagram is explained on the right.

D – The top row shows the results of five sets (Models 1-5) of simulations of microcircuit parameter changes and their similarity to the rsEEG changes in θ, β and γ bands in PScz (the model does not produce an α peak). The parameters changed in each model are illustrated in the microcircuit schematics for Models 1-5 (bottom row): parameter increases are denoted by whole lines and decreases by dotted lines. Each model is used to produce 10 simulations, starting with standard parameter values (to simulate Con) plotted in dark blue, and then reducing or increasing the parameters illustrated below in increments of 3% to simulate PScz (up to the most extreme change, plotted in dark red). Only Model 5 – a increase in superficial pyramidal self-inhibition, i.e. a loss of synaptic gain – reproduces the changes seen in all three frequency bands.

Figure 3 – MMN data and modelling analysis

A – Mismatch difference waves (i.e. deviant–standard, mean ±s.e.m.) for Con (n=94; blue), PScz (n=96; red) and Rel (n=42; green) at electrode Fz. Group differences are computed using *t*-tests (uncorrected) at each timepoint and are marked with red (PScz vs Con) and green (Rel vs Con) bars above the difference waves. There were no significant PScz vs Rel differences.

B – The lower plot shows the location of the mismatch effect (i.e. deviants – standard) at sensor level across all Con and PScz, displayed at $P<0.05$ (FWE). Fz is shown in white. The peak effect is shown in green: $P<0.001$ (FWE), $t(376)=11.23$. The upper plot shows sensors vs time: the peak effect occurs at 198 ms.

C – These plots show the interaction of condition and group for the Con > PScz contrast (left) and Con > Rel contrast (right) in the same format as Fig 2B, at the lower threshold of $P<0.005$ (unc) for display purposes. Both groups demonstrate similar differences from controls in the mismatch contrast in frontocentral sensors just before 200 ms.

D – Microcircuit models were compared, differing only in which parameters were allowed to change from their priors (estimated G connectivity parameters are shown, as in Figure 2C). These models' free G parameters included various combinations of superficial (sp) and/or deep (dp) pyramidal cell (blue) connections to or from inhibitory interneurons (ii, red), and self-inhibition of sp and ii cells. Note that each parameter – within each microcircuit – could differ between subjects but was constrained to be the same in every cortical area within subjects, except for sp self-inhibition which could differ throughout. The final model also estimated delay D and time constant T parameters (these were fixed in the other five models).

E – Model comparison and evaluation. Left: The protected exceedance probability is the probability a particular model is more likely than any other tested model, above and beyond chance, given the group data. The model with most free parameters is at the far right; it comes second to the 6G model with fixed delays (D) and time constants (T) and 6 microcircuit connectivity parameters estimated.

Right: A histogram of R^2 values for all participants for the winning model: it fits most participants well.

F – A PEB analysis of MMN model parameters (i.e. connections) that contribute to the PScz > Con mismatch effect. The results are plotted on the left (with 95% Bayesian confidence intervals) and shown in schematic form on the right; parameters with posterior probabilities of $P>0.95$ or $P>0.99$ of contributing to the group difference effect are indicated with one or two asterisks (respectively). On the plot, self-inhibitory connections are shaded grey, forward

connections shaded yellow, and backward connections shaded purple (matching the colours in the schematic). The y axis denotes log-scaling of the effect size: changes of exp(±0.2) are of roughly ±20%. Some parameters have been eliminated during Bayesian model reduction (see Supplement). The analysis indicates PScz showed greater self-inhibition (or reduction in synaptic gain) in bilateral IFG in the mismatch contrast. The Rel > Con contrast did not show significant effects.

G – A PEB analysis of MMN mismatch effect model parameters that correlate with current ('state') abnormal auditory percepts within PScz only, plotted in the same format as Figure 3F. Within PScz, abnormal auditory percepts relate to reduced self-inhibition in right IFG, but disinhibition in left IFG (in Broca's area).

N.B. All effects shown in F and G are also present without the addition of age, sex, and smoking covariates (P>0.95). Inclusion of a chlorpromazine dose equivalent covariate renders the analysis in 3F non-significant (P>0.75), but it makes the overall effect of PScz on L & R IFG self-inhibition become significant (see Figure S4C).

Figure 4 – 40 Hz ASSR data and modelling analysis

A – 40 Hz ASSR time courses at electrode Fz for Con (n=92; blue), PScz (n=94; red) and Rel (n=42; green). 16 clicks were played at 40 Hz, starting at 0 ms. Group differences in the baseline deflection (not modelled subsequently) emerge after around 250 ms: shown with red bars (Con vs PScz) and green bars (Con vs Rel), both $P<0.05$ (*t*-tests per timepoint, uncorrected).

B – γ (35-45 Hz) frequencies with the strongest power (in the normalized spectrum) in each participant are shown in a histogram.

C – These normalised time frequency plots show the ~40 Hz responses around 100-400 ms. The PScz and Rel plots have areas of difference from Con encircled in black; the Rel plot has areas of difference from PScz encircled in white ($P<0.05$ *t*-tests at each time and frequency).

D – The left plots show the bilateral A1 (transverse temporal gyrus) sources chosen following source localization: [±50 -12 4]. The 40 Hz ASSR model structure is on the right: bilateral sources in A1.

E – Left: To improve the DCM fit of the cross spectral densities in bilateral A1 in this non-standard paradigm, we used empirical priors (also see Figure S1A) for: J(1), the contribution spiny stellate cells make to the EEG signal; S, the gain of the neuronal activation function; T, population time constants; and also w, the width of the ~40 Hz Gaussian bump. The plot shows that the Full model (with all the empirical priors) is superior to other models that used standard values for their respective priors (or for '-w', 1 Hz instead of 4 Hz). Right: a histogram of R^2s for all participants for the winning model.

F – PEB analysis indicated PScz+Rel > Con showed increased neural transmission delays in L A1.

G – Left: PEB analysis (in the same format as Figure 3H) indicated PScz+Rel > Con (a psychosis 'genetic risk' effect) had decreased sp-ii connectivity. Right: PScz > Rel (a psychosis 'diagnosis' effect) shows decreased sp self-inhibition in bilateral A1.

H – PEB analysis in PScz, showing abnormal auditory percepts are associated with disinhibition of the sp-ii circuit (and increased sp self-inhibition in L A1).

All effects shown in F, G, H and I are also present without the addition of age, sex and smoking covariates ($P>0.95$), and also with inclusion of chlorpromazine dose equivalents as a covariate.

Figure 5 – Resting state fMRI modelling analysis

A – For comparative purposes, the rsfMRI connectivity analysis was conducted on the same network as the MMN analysis. Results for Con (n=85) and PScz (n=72) are shown in the same format as Figure 3F. As in the MMN, PScz showed increased self-inhibition in bilateral IFG. Inclusion of chlorpromazine equivalent dose as a covariate still showed increased self-inhibition in L IFG but only at $P>0.75$.

B – rsfMRI connectivity analysis without covariates for Con (n=85) and Rel (n=45) is shown. Like PScz, Rel show increased self-inhibition in bilateral IFG, but this effect disappeared with addition of the age covariate ($P<0.75$).

C – Left: Within PScz, abnormal auditory percepts ('trait' measure) related to increased self-inhibition in bilateral IFG.

Right: Conversely, abnormal auditory percepts ('state' score – i.e. experiences within the last week only) relates to disinhibition in temporal areas and also a loss of top down connections within auditory cortex. The R A1 effect was attenuated if age, sex, and smoking covariates were not included, and if a chlorpromazine dose equivalent covariate was added.

D – Left: Within PScz, BPRS positive symptom score related to disinhibition throughout the MMN network and increased forward connectivity in 3/4 connections. Most effects were robust to addition of chlorpromazine dose equivalents as a covariate (all $P>0.99$ except L IFG self-inhibition, $P>0.75$), removal of the hallucinations score from the BPRS positive symptom total (all $P>0.95$ except L IFG and R A1 self-inhibition, $P>0.75$), and analysis without covariates (all $P>0.99$ except L IFG self-inhibition, $P>0.75$).

Right: Within PScz, BPRS negative symptom score related to disinhibition in temporal nodes of the MMN network.

All effects shown (except Rel > Con) are also present without the addition of age, sex and smoking covariates, and also if participants (2 controls, 8 PScz) with rsfMRI SNR <25 are excluded (all $P>0.95$). Some rsfMRI results are no longer significant without GSR (Figure S7). No results change substantially with inclusion of chlorpromazine dose equivalent as a covariate unless stated.

Figure 6 – Summary of key findings across paradigms

This figure illustrates similar DCM findings across paradigms using the schematic illustrations from previous analyses. The inset at bottom right shows the canonical microcircuit model for EEG (below), which exists in each modelled cortical area (above). The microcircuit consists of superficial and deep pyramidal cells (sp and dp, blue), inhibitory interneurons (ii, red), and spiny stellate cells (ss, green), interconnected with excitatory (arrowheads) and inhibitory (beads) connections.

A – Crucially, the PScz group consistently exhibited increased self-inhibition (as expected from a loss of synaptic gain) – in superficial pyramidal cells in particular (i.e. in the EEG paradigms). This was the case (from left to right) in A1 in the 40 Hz ASSR (when compared with Rel), in bilateral IFG in both the MMN (deviant–standard contrast) and the resting state fMRI, and in the rsEEG simulations.

B – Within the PScz group, abnormal auditory percepts were linked with disinhibition in A1 in both the 40 Hz ASSR paradigm and the resting state fMRI, and with disinhibition in L IFG – i.e. Broca's area – in the MMN (deviant–standard contrast).

EEG – Resting s

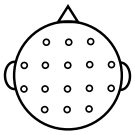

Preprocessing (EEGLAB & SPM): channel & epoch rejection, ICA component rejection (Multiple Artefact Rejection Algorithm), giving spectra from Con (n=98) and Scz (n=95).

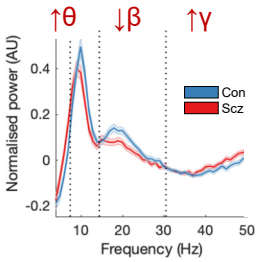

Analysis of group differences in power spectrum frequency bands

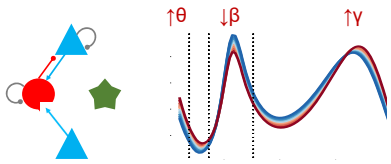

Microcircuit model used to simulate power spectrum differences (no model fitting to individual subjects)

EEG – Mismatch Negativity (MMN)

Preprocessing (EEGLAB & SPM): channel & epoch rejection, ICA component rejection (Multiple Artefact Rejection Algorithm), giving MMN from Con (n=93), Scz (n=95) and Rel (n=40).

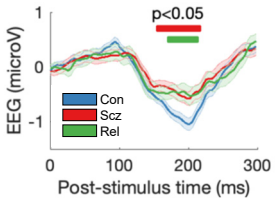

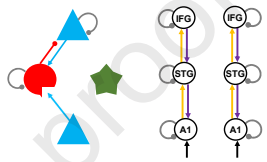

Group differences in mismatch responses found. Bilateral MMN network source priors for MMN (bilateral A1, superior temporal & inferior frontal gyri) taken from previous EEG, MEG & fMRI literature (Garrido et al (59)). Dynamic causal modeling for evoked response potentials performed using different canonical microcircuit models and group empirical Bayesian fitting, then model comparison.

EEG – Auditory steady state response at 40 Hz (40 Hz ASSR)

Preprocessing (EEGLAB & SPM): channel & epoch rejection, ICA component rejection (Multiple Artefact Rejection Algorithm), giving spectra from Con (n=92), Scz (n=94) and Rel (n=42).

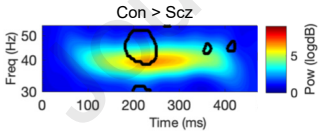

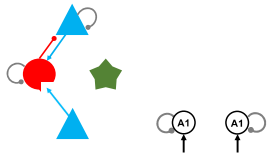

Group differences in 40 Hz power and frequency found. Bilateral A1 [±50 -12 4] prior (from group γ source localization) used to reconstruct virtual electrode data. Dynamic causal modeling for cross spectral densities performed using the winning canonical microcircuit model structure from the MMN; also model comparison of alternative priors.

fMRI – Resting state (rsfMRI)

Preprocessing (FreeSurfer): conversion to CIFTI, regression of global signal, motion scrubbing, cortical parcellation (Glasser et al. 2016), giving rsfMRI from Con (n=85), Scz (n=72) and Rel (n=45).

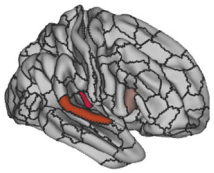

Spectral dynamic causal modeling analysis of endogenous interactions between MMN network sources (bilateral A1, superior temporal & inferior frontal gyri) using group empirical Bayesian fitting

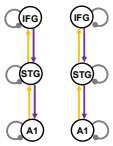

Scz > Con

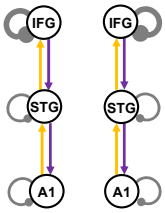

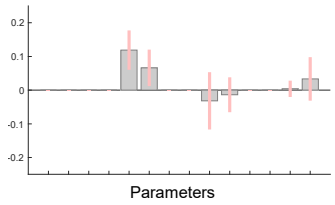

Analysis of group and individual differences in dynamic causal modeling parameters (± age, sex & smoking covariates) within and across paradigms using parametric empirical Bayes

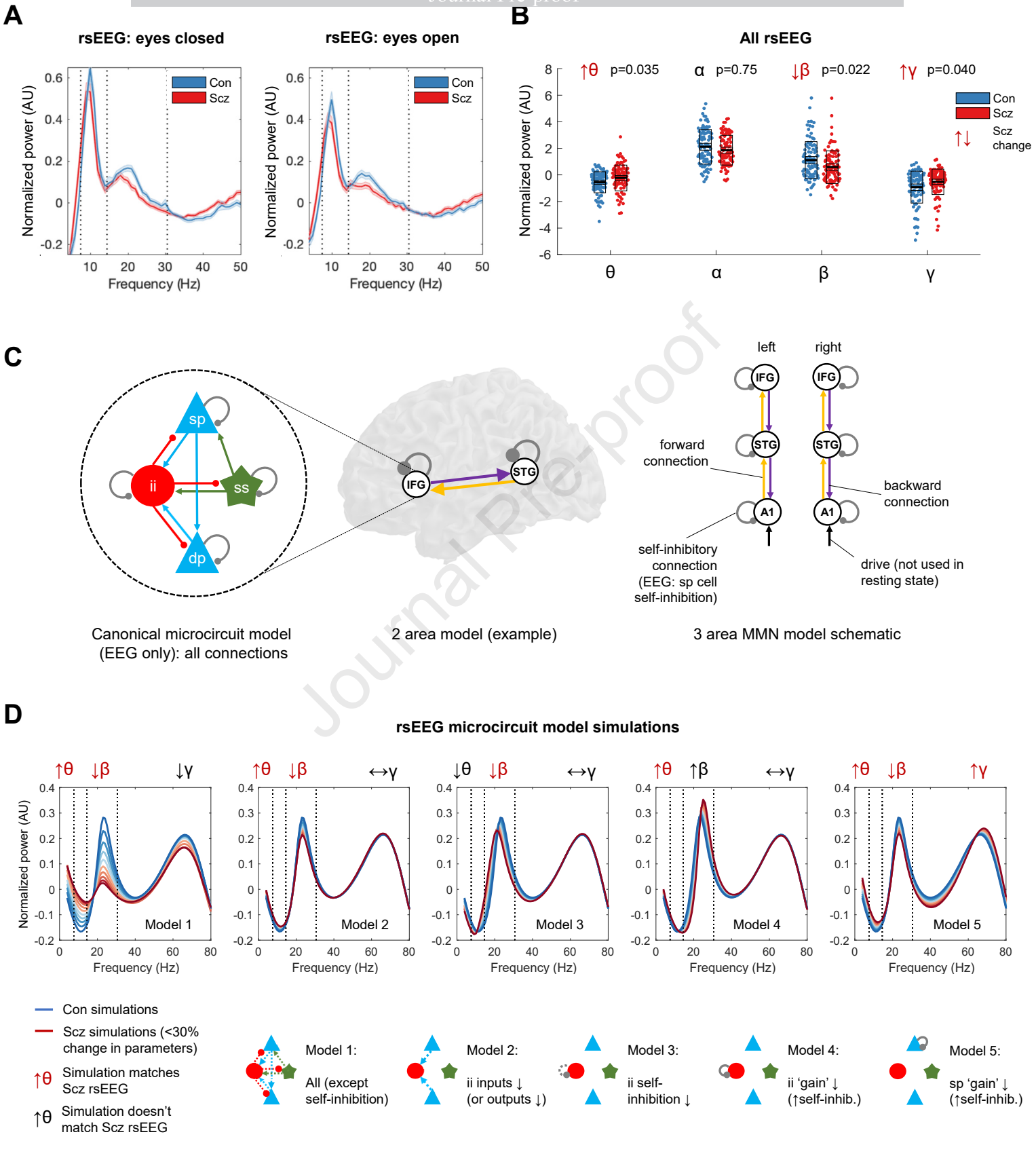

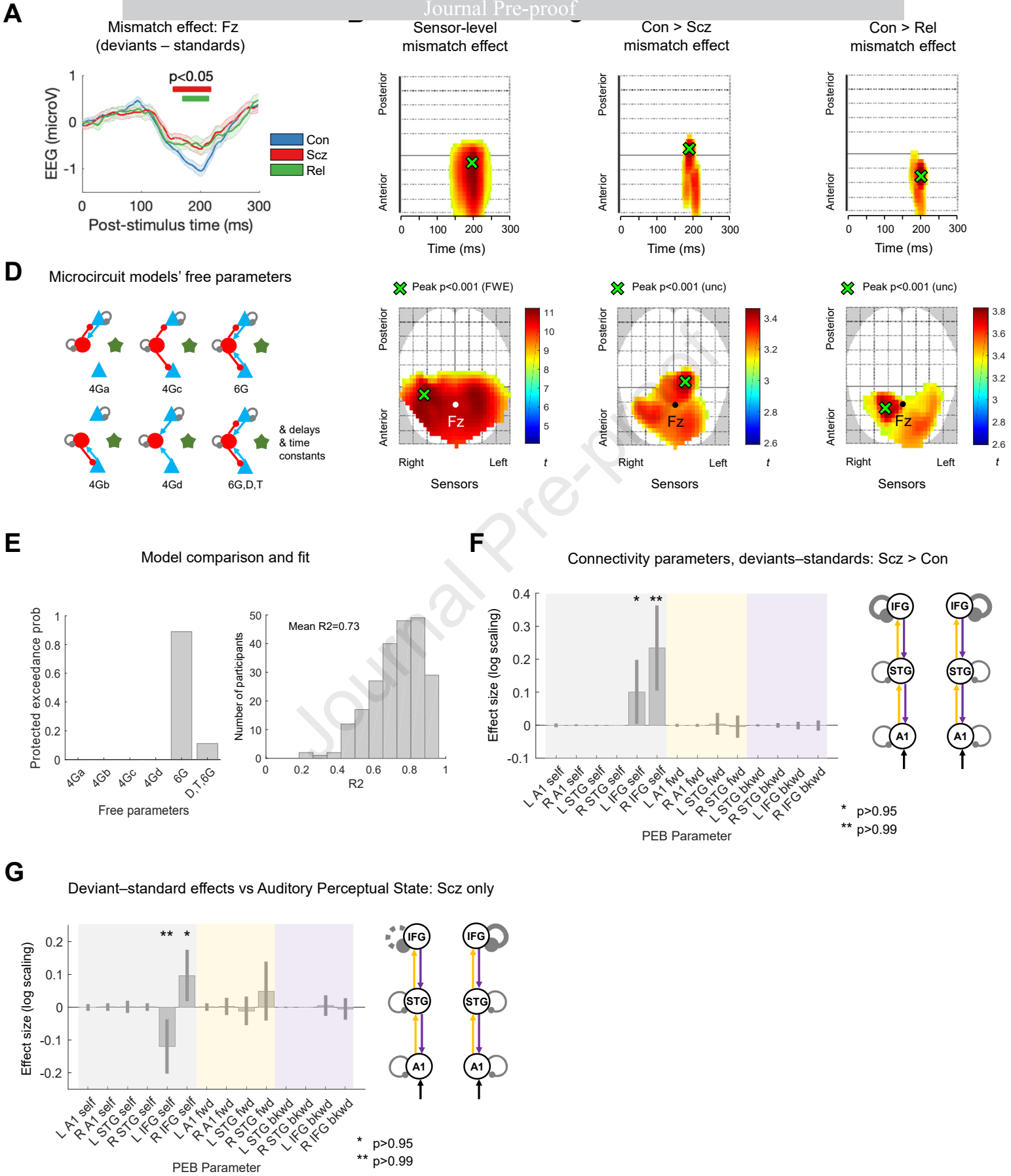

A

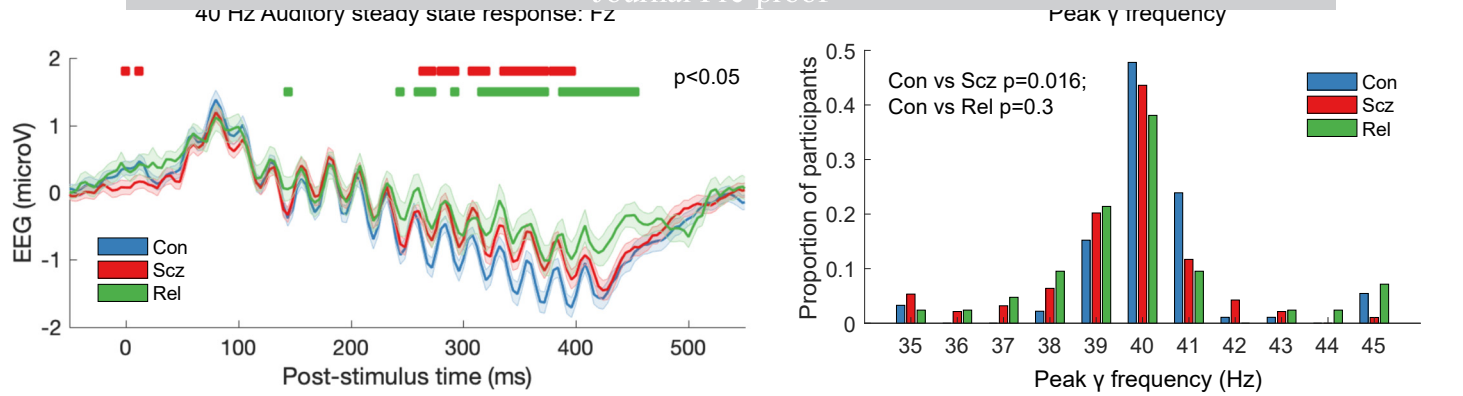

C

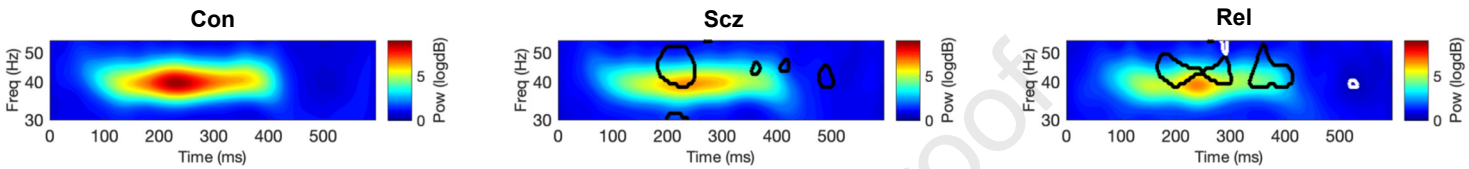

D

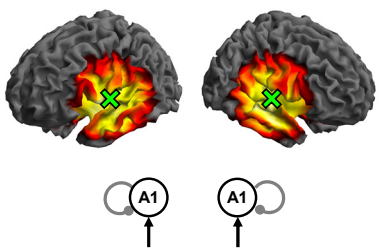

E

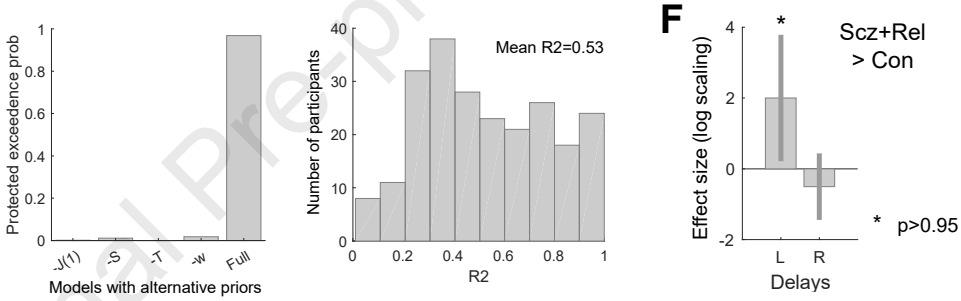

F

G

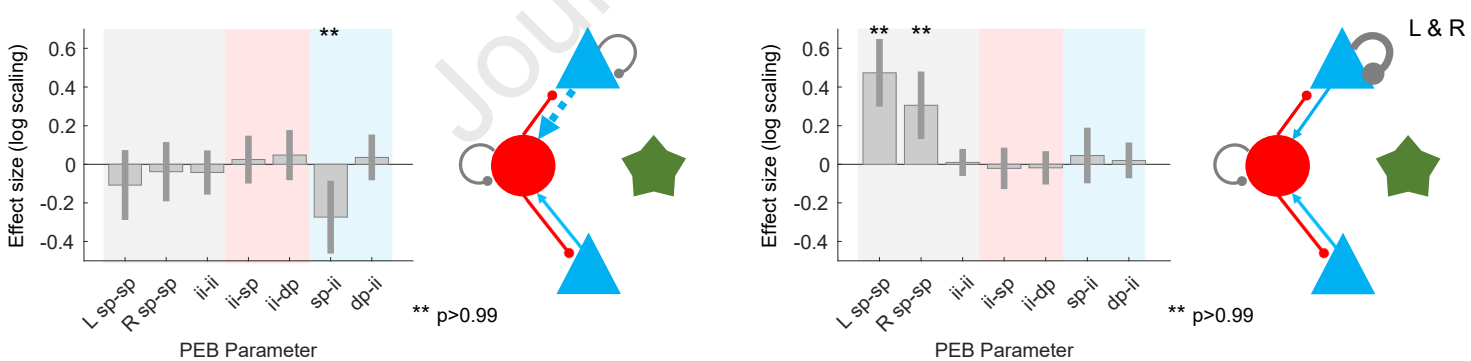

H

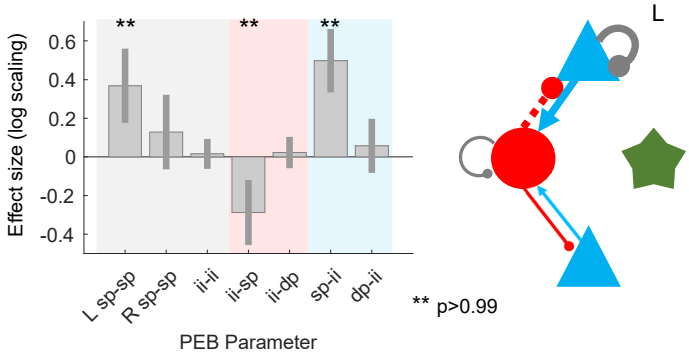

A

rsfMRI connectivity parameters: Scz > Con

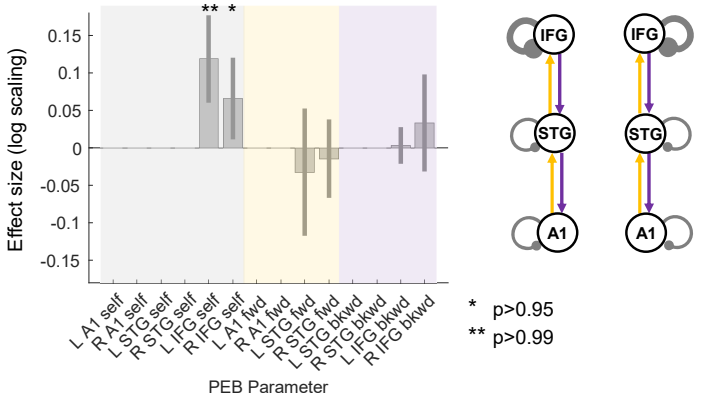

B

rsfMRI connectivity parameters: Rel > Con

(without age covariate)

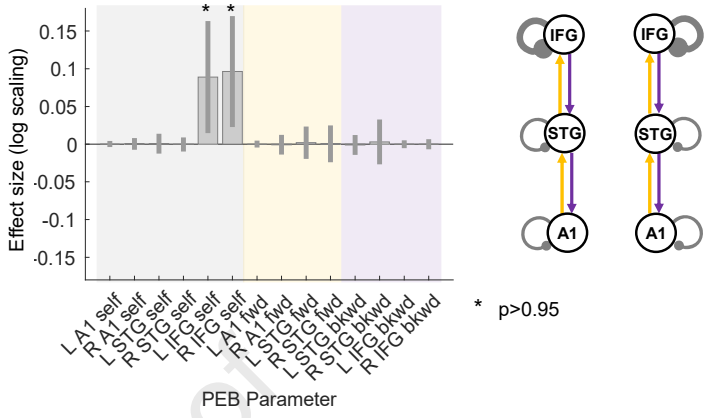

C

rsfMRI connectivity parameters vs

Auditory Perceptual Trait Score: Scz only

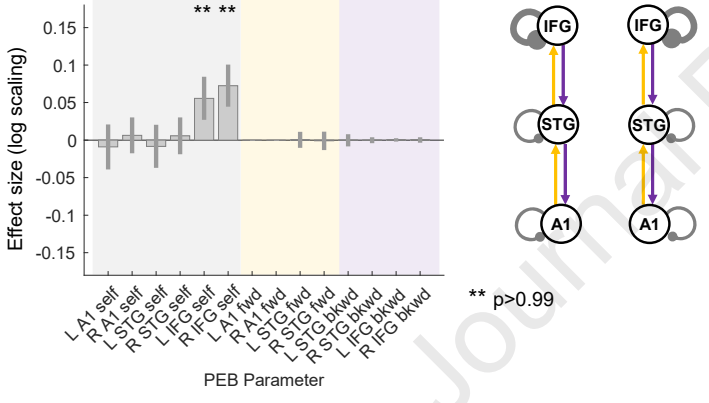

rsfMRI connectivity parameters vs

Auditory Perceptual State Score: Scz only

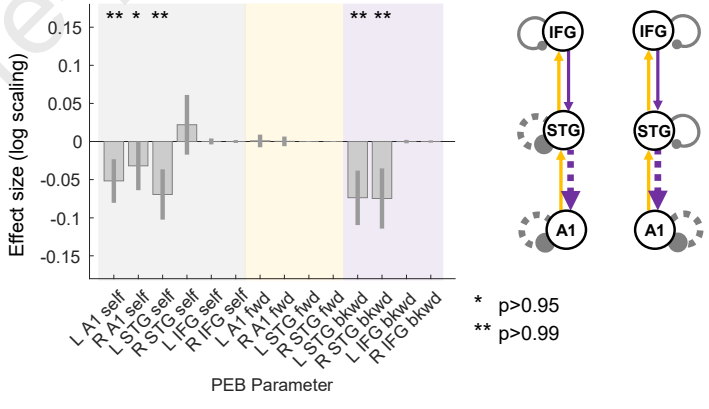

D

rsfMRI connectivity parameters vs positive symptoms:

Scz only

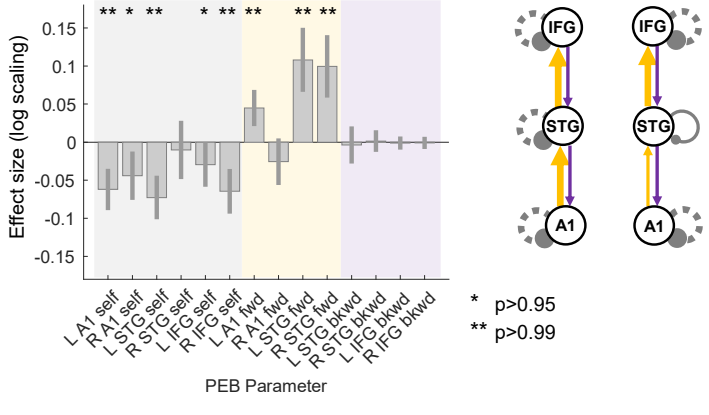

rsfMRI connectivity parameters vs negative symptoms:

Scz only

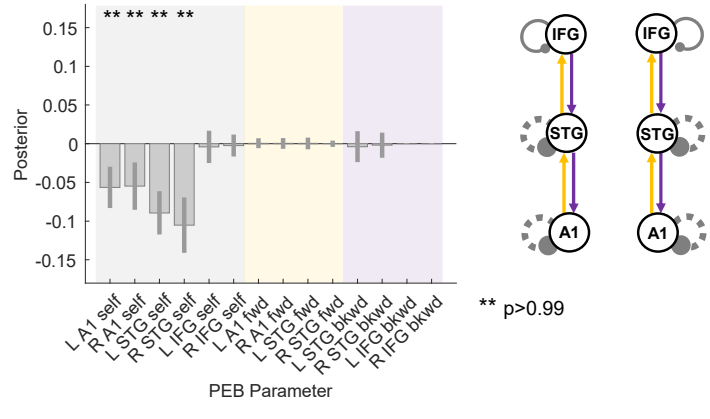

A

Scz show increased self-inhibition – indicating loss of (pyramidal) synaptic gain – vs other groups

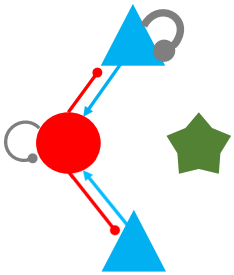

Scz simulations, rsEEG

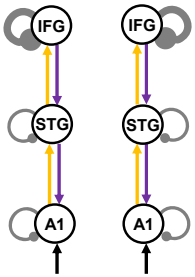

Scz > Con, MMN

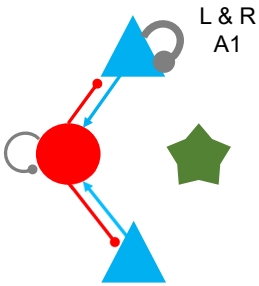

Scz > Rel, 40 Hz ASSR

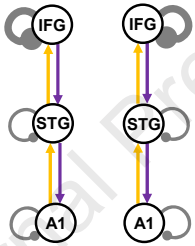

Scz > Con, rsfMRI

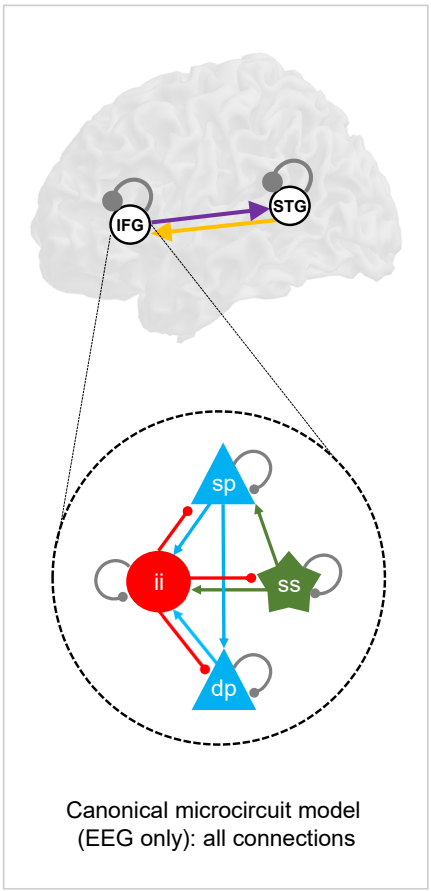

Canonical microcircuit model
(EEG only): all connections

B

Abnormal auditory perception (AP) in Scz linked to disinhibition in auditory/speech areas

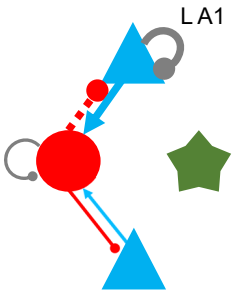

Scz & AP Trait, 40 Hz ASSR

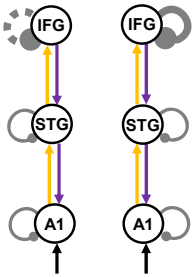

Scz & AP State, MMN

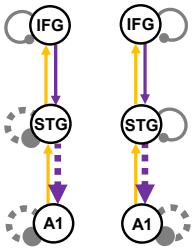

Scz & AP State, rsfMRI